# Electric Machine Bearing Health Monitoring and Ball Fault Detection by Simultaneous Thermo-Mechanical Fibre Optic Sensing

Anees Mohammed and Siniša Djurović

***Abstract*—This article reports the use of fiber Bragg grating (FBG) sensors for electric machines' in-service bearing condition monitoring. The proposed method enables simultaneous extraction of thermal and mechanical information on the bearing operational status for health monitoring and fault diagnosis purposes. The work first reports the instrumentation, calibration and the measurements interpretation methods of an FBG array sensor fitted to the drive-end bearing of an operating inverter driven induction motor. Experimental tests are then undertaken on a purpose build test rig to evaluate the proposed in-situ sensing scheme's performance under healthy and faulted bearing conditions. The results demonstrate that the measurements acquired by individual FBG sensors fitted in the bearing architecture contain concurrent thermal and mechanical information, which can be clearly differentiated to enable understanding of the examined motor bearing's thermal only and mechanical only operating conditions. Furthermore the in-situ measurements obtained in fault conditions are shown to contain clearly defined time and frequency domains fault signatures, which can enable unambiguous fault diagnosis and trending.**

***Index Terms*—Bearings, electric machines, fault diagnosis, fiber bragg grating sensor, temperature and strain monitoring.**

## I. Introduction

BEARINGS are vital enablers of the electro-mechanical energy conversion process in electric machines. They are recognized to be the component with one of major failure rates in in-service machinery [1]. Generally, undetected bearing failures will result in loss of availability, and are often accompanied by irreversible damage and/or high maintenance cost. Machine bearing structure monitoring is therefore important to ensure their reliability and availability [2]. The root causes of bearing failure are found in the mechanical and thermal stresses imposed on their structure during operation and in contemporary inverted-driven machinery in particular increasingly include electrical erosion [1]–[3]. In this respect, the variable speed nature of the growing renewables and transportation power conversion applications is particularly likely to impose highly dynamic operating conditions and thus increase the significance of effective understanding of bearing in-service stresses.

The prevailing practical method for bearing health monitoring and fault diagnosis is based on machine frame vibration analysis using accelerometers and/or bearing temperature monitoring by means of conventional thermal sensors [1], [4]. This is because bearings, whether healthy or faulty, inherently generate mechanical and thermal excitation whose nature will change with fault presence and can thus be monitored for diagnostic purposes [4]. Capturing these changes as clearly and as early in the fault development process as possible can enable improved efficacy diagnosis. This is an area where improved methods that allow for sensing point placement nearer to the actual bearing structure/points of failure, for in-situ observation of high fidelity, fault exclusive, signature could offer considerable advantages over the existing monitoring techniques. Further improvements could be attained by addressing the electro-magnetic interference (EMI) immunity constraints of current monitoring techniques where reliable measurements are required [5].

Fibre optic sensing has emerged as a promising alternative for electric motor condition monitoring: its application for machine mechanical and thermal monitoring [5]–[12] is attracting increased interest. FBG sensing technology, with its advanced features such as small size, EMI immunity, multiplexing and multi-physical sensing presents an attractive proposition for enabling targeted in-situ monitoring of bearing multi physical operating conditions. The FBG sensor cost is currently comparable to cost of sensors conventionally used in electric machine applications, but the required FBG interrogator systems are costly. FBG multiplexing and multi-physical sensing features are key in enabling sensing system cost reduction for advanced electric machine monitoring applications: multiplexing facilitates distributed embedded sensing schemes where a single fibre can carry an array of distributed sensing points, while multi-physical sensing can enable a comprehensive sensing system design where individual sensing points can monitor different physical measurands where required [7], [10].

FBG sensing application for electric machine bearings monitoring is only starting to be examined, with very recent reports suggesting encouraging potential for this application [13]–[17]. However, these studies largely focus on strain monitoring only

Manuscript received September 26, 2019; revised January 14, 2020 and April 4, 2020; accepted May 11, 2020. Date of publication June 19, 2020; date of current version February 19, 2021. This work was supported by the UK Engineering and Physical Sciences Research Council (EPSRC) HOME-Offshore: Holistic Operation and Maintenance for Energy from Offshore Wind Farms Consortium under Grant EP/P009743/1. *(Corresponding author: Siniša Djurović.)*

The authors are with the School of Electrical and Electronic Engineering at University of Manchester, Manchester M13 9PL, U.K. (e-mail: anees.mohammed@manchester.ac.uk; sinisa.durovic@manchester.ac.uk).

Color versions of one or more of the figures in this article are available online at https://ieeexplore.ieee.org.

Digital Object Identifier 10.1109/TEC.2020.3003793

[13]–[16], and are performed on standalone bearings, where sensing is implemented within the bearing housing and not on the actual bearing geometry within an operating electric machine. [13] examines bearing structure in-situ sensing application but does not provide information on the used application technique nor full interpretation of obtained results. Rotary bearing FBG sensing applications in operating electric machines require further work to be understood and optimised, with a particular focus on exploring requirements for effective application of single point multi-physical sensing for condition monitoring purposes. The authors' recent study [17] examines the potential for use of FBG sensing to attain in-situ multi-physical monitoring in a single point of a healthy electric machine bearing operated at nominal conditions. This paper further explores the in-situ FBG sensing application for condition monitoring bearings of operating electric machines to provide full detail of the methodology devised to simultaneously extract multi-physical measurands and examine FBG multiplexing application. Furthermore, an extensive experimental study is undertaken to assess the proposed monitoring technique's performance in an inverter driven machine operating without and with a faulted bearing (progressive rolling element fault), including analysis and understanding of the novel diagnostic indices provided by in-situ multi-physical sensing, and localised dynamic strain in particular, and an analysis of the applicability of in-situ sensed multi-physical features for diagnostic purposes in general and in separate locations.

To this end, the paper reports a study of FBG usage for in-situ multi-point monitoring of simultaneous thermal and mechanical operating conditions of an in-service squirrel cage induction motor (IM) bearing structure in healthy and rolling element fault conditions. For this purpose, the drive end bearing of a commercial test IM was instrumented with an FBG array sensor operated by a commercial interrogator platform. The sensor design, application and calibration procedure, and the method for extracting multi-physical parameter information from the measurements are detailed in the study. To examine and verify the proposed method's potential to provide useful multi domain information on the healthy and faulted bearing operating status, a range of experiments are undertaken in different mechanical and thermal operating conditions on a purpose built IM laboratory test-rig. It is found that the reported method enables recognition of both thermal and mechanical operating conditions relevant to diagnostic purposes that are sensed in a given monitoring point by a single FBG head. The bearing ball fault was shown to be clearly detected and its severity trended by the FBG array sensing system measurements containing evident fault signature in both time and frequency domains. The reported technique offers a considerable advantage over the standard vibration measurement based bearing condition monitoring, by allowing monitoring of both in-situ thermal and mechanical conditions in the bearing structure through application of a single sensor. This cannot be achieved using conventional vibration sensing platforms that only observe mechanical domain related phenomena and require additional thermal monitoring devices for observation of bearing thermal conditions.

TABLE I
TEST MOTOR SPECIFICATION

| Motor Data | |
|---|---|
| Rated Power / Voltage / Current | 0.55 kW / 400 V / 1.6A |
| Efficiency | 66 %, IE1 |
| Rated speed | 1380 rpm |
| Cooling method | IC 411 |
| Insulation/Temperature rise class | F / B |
| Bearing type | NSK 6202 |
| Design standard | IEC- 60034 |

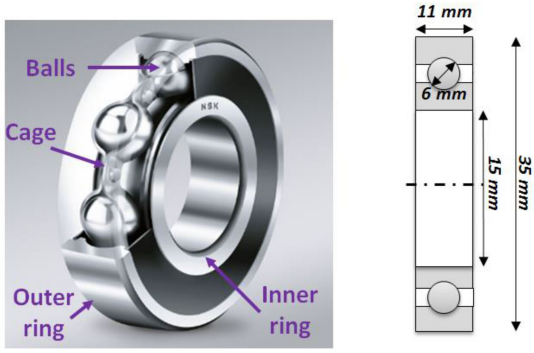


(a) NSK-6202 bearing strcture and dimensions

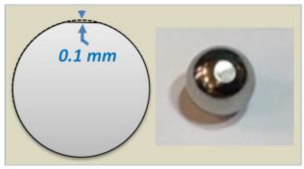


(b) 0.1 mm ball fault

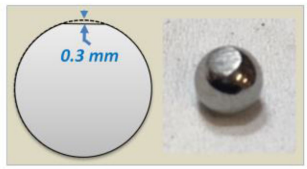


(c) 0.3 mm ball fault

Fig. 1. Examined bearing design and ball fault conditions.

## II. TEST BEARING DESIGN

The studied ball bearing is an NSK-6202 single row deep groove design that is factory fitted to the commercial test IM [18]. The test motor specifications are shown in Table I. Fig. 1(a) shows the examined bearing structure and dimensions: it contains eight balls uniformly placed between the inner and the outer ring. The inner ring is fitted to the rotor shaft and rotates with the rotor structure at rotor angular velocity. The outer ring is fitted to the motor end-cap and remains stationary in operation. The uniform spacing between balls is maintained by a bearing cage which rotates at identical speed of rotation to that of the balls.

In general, bearing faults are classified depending on their location in the bearing structure as: outer race faults, inner race faults, rolling element faults and cage faults [1]–[3]. For the purpose of evaluating the use of FBG sensing design for bearing fault diagnosis proposed in the following section, a single rolling element (i.e. ball) fault was experimentally emulated in this work. This was achieved by machining healthy balls disassembled from an identical bearing to remove 0.1 mm and 0.3 mm of their diameters, as shown in Figs. 2(b) and (c). This allowed two separate levels of single rolling element fault to experimentally be emulated by fitting the individual damaged balls within the test bearing.

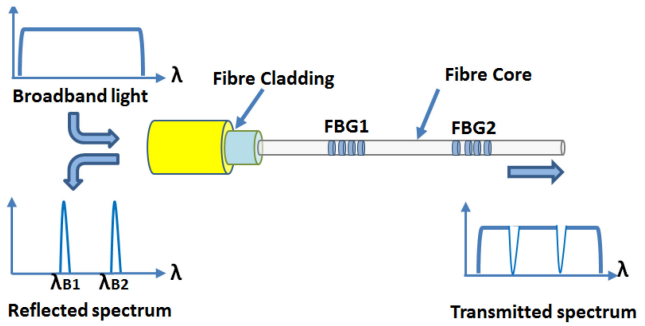


Fig. 2. FBG strcture and sensing principal.

## III. Proposed FBG Sensing System Operation, Design and Installation Principles

### A. Fibre Bragg Grating Sensor Operating Principles

An FBG sensor is a micro structure imprinted into the core of a standard single-mode optical fibre; a single imprint is referred to as an FBG head. It is formed longitudinally on the optical fibre core in a length typically of the order of a few millimeters, in which a modulated periodic refractive index is formed in a fibre core when exposed to an interference pattern of ultraviolet laser light [5]. Fig. 2 illustrates the structure and the fundamental operating concept of an FBG sensing system. The fibre containing an FBG heads is illuminated with broadband light, each FBG reflects a specific light spectrum that matches its designed Bragg wavelength. The process of fibre light excitation and examination of the reflected spectrum for Bragg wavelengths is managed by an interrogator unit [17].

The basic operation principle of FBG sensing is to monitor the narrowband reflected Bragg wavelength after injecting broadband light into the optical fibre. The base Bragg wavelength, $\lambda_{\mathrm{B}}$, can be defined by [5]:

$$\lambda_{\mathrm{B}} = 2\,\Lambda\, n_{eff} \tag{1}$$

where: $\Lambda$ is the FBG gratings pitch and $n_{eff}$ is the effective index of the optic core. These parameters alter with the change in strain and/or temperature the FBG is exposed to, in turn altering the reflected Bragg wavelength. The reflected $\lambda_B$ relative rate of change due to changes in the FBG structure parameters can be defined in terms of the acting thermal and/or mechanical excitation as [17]:

$$\frac{\Delta}{\lambda}_{\mathrm{B}} \lambda_{\mathrm{B}} = k_\varepsilon\,\Delta\varepsilon + k_T\,\Delta T$$

$$\text{where}: \; k_\varepsilon = \left(\Lambda\frac{dn_{eff}}{d\varepsilon} + n_{eff}\frac{d\Lambda}{d\varepsilon}\right), \tag{2}$$

$$\text{and } k_T = \left(\Lambda\frac{dn_{eff}}{dT} + n_{eff}\frac{d\Lambda}{dT}\right)$$

In (2): $\Delta\lambda_B$ is the shift in the Bragg wavelength, $\Delta\varepsilon$ is the change in strain, $\Delta$T is the change in temperature and $k_\varepsilon$ and $k_T$ are the FBG sensitivity factors to strain and temperature, respectively. $k_\varepsilon$ signifies the Bragg wavelength shift caused by elastic-optic effect due to strain while $k_T$ describes the Bragg wavelength variation due to thermo-optic and thermal expansion

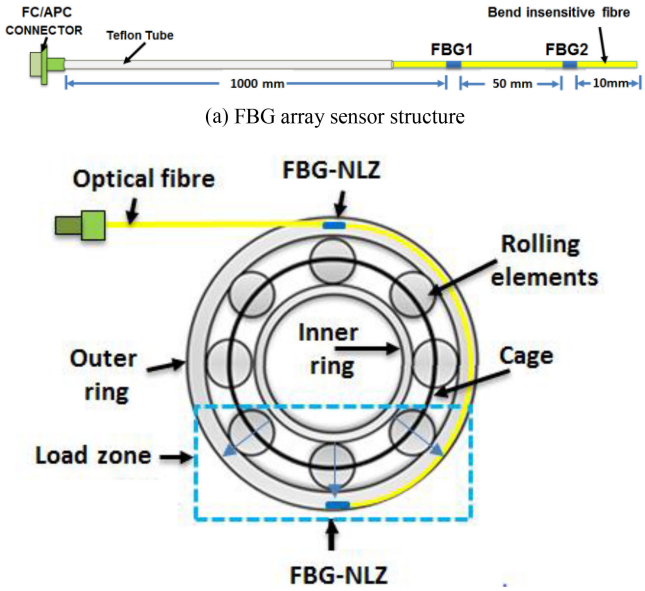


(a) FBG array sensor structure

(b) Bearing structure cross-section and FBG heads location

Fig. 3. Bearing instrumentation with the FBG sensing system.

effects caused by temperature variation. A standard FBG has sensitivity to mechanical strain of $\approx$ 1.2 pm/$\mu\varepsilon$ and to thermal excitation of $\approx$ 12 pm/°C [5], [12]. However, the FBG sensitivity factors are in principle design dependant and can, for example, vary with packaging and bonding methodologies; these values are best determined in characterisation tests for a particular application [9].

### B. FBG Sensor Design and İnstallation

The target FBG sensing application is simultaneous thermal and mechanical conditions monitoring in a single point on the bearing's stationary structure. The outer ring temperature and dynamic deformation (strain) are aimed to be measured and the usability of these measurements for bearing health condition monitoring evaluated. To this end, an FBG array sensor was designed and prototyped to be installed on the examined IM's drive end bearing outer ring.

Fig. 3(a) shows a schematic diagram of the array sensor design: it contains two FBG heads imprinted in a polyimide single mode optical fibre. The FBG heads' length is 5 mm and their respective central Bragg wavelengths are 1533.730 nm and 1548.120 nm. The spatial distribution of the FBG heads within the fibre array is designed to enable positioning one sensing point in the test bearing load-zone (FBG-LZ) and the other in its non-load zone (FBG-NLZ). This is done to enable investigation of different FBG sensing locations for bearing health diagnosis. Fig. 3(b) shows the FBGs positions in the examined bearing outer ring structure.

For the purpose of embedding the FBG array sensor, the test bearing was disassembled and a 0.5 $\times$ 0.5 mm groove machined on its outer ring surface in circumferential direction. The optical fibre containing the FBG sensing heads was then embedded into the machined groove and bonded to the outer ring structure by means of strain gauge glue. Finally, the FBG

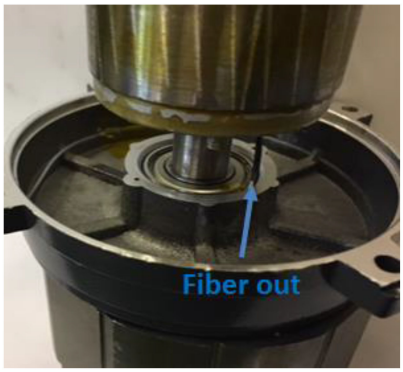


Fig. 4. End-cap housing installed bearing embedded with the sensor array.

sensors instrumented bearing was assembled, mounted on the rotor shaft and installed into the end-cap housing, as shown in Fig. 4. Furthermore, this procedure enables secure location of the FBG array in the examined bearing's outer ring during the assembly and disassembly process required for practical emulation of the rolling element fault.

## IV. Measurements and Sensor Calibration

The FBG sensing technology is inherently thermo-mechanically cross sensitive: a single FBG head can be designed to enable simultaneous or exclusive temperature and/or strain measurements. This feature is used in this study to enable each FBG in the array to simultaneously sense temperature and strain of the bearing outer ring structure.

The discrimination between temperature and strain related measurements in the observed FBG wavelength shift in this application is based on: **1)** the intrinsic substantial excitation frequency difference, as governed by electric machine multi-physics, i.e. a relatively high excitation frequency for mechanical excitation (strain) and a low excitation frequency for thermal excitation [2]; **2)** the variation band width, which is limited for excitation arising from monitored strain due to the rigid bearing structure; and **3)** the inherent significant difference between FBG strain and temperature sensitivity [1].

The general procedure for conversion of bearing in-situ multi-physical FBG measurements into information on its thermal and mechanical operating conditions is illustrated in the flowchart in Fig. 5. Once the FBG array is installed in the bearing, it is thermally calibrated within the bearing structure to determine its thermal sensitivity (i.e. wavelength-temperature fit curves). This is achieved by inserting the sensor embedded bearing in a thermal chamber and exposing it to a series of static thermal excitation steps in the examined bearing's thermal operation range of 25 to 115 °C. The wavelength reflected by each FBG is recorded along with the chamber temperature for each considered excitation level, and then used to calculate the sensors' thermal fit curves.

During measurement, the interrogator sends broadband light to the FBG array and receives the reflected Bragg wavelength from each of its FBG heads, containing both thermal and mechanical information. The reflected wavelengths are then

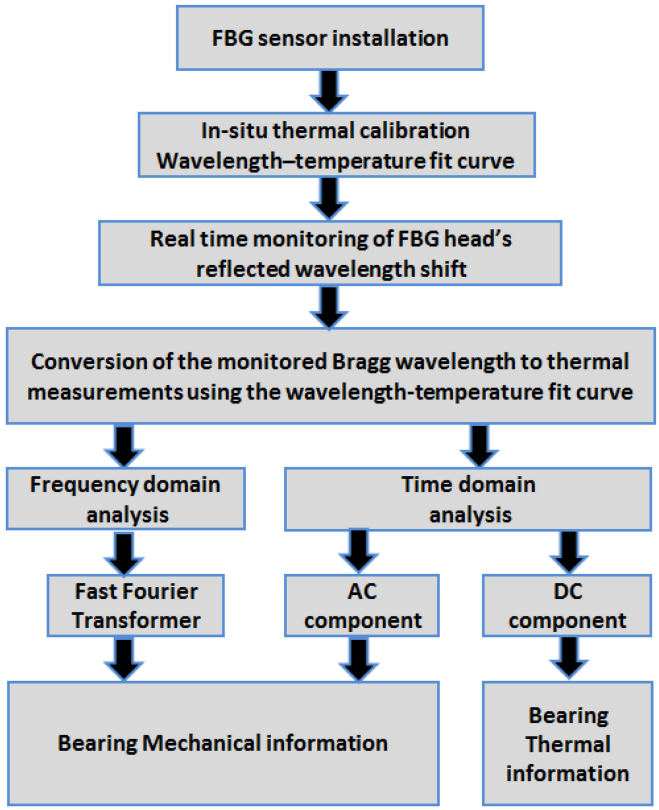


Fig. 5. The proposed thermo-mechanical measurement process flowchart.

thermally scaled using the determined fit curves and the resulting measurements then processed to extract thermal and mechanical information: in the time domain, the average value (DC component) of the thermally scaled measurements represents the bearing temperature; the dynamic variation (AC components) in the thermally scaled measurements however directly relates to the measured outer ring dynamic deformation induced by the rolling elements passing the FBG head's position, and therefore represents a relative strain measurement. The AC content is thus proportional to relative strain and can therefore provide information on the bearing's mechanical conditions, including ball and cage health. The frequency domain analysis is executed in a $2^{17}$ rectangular window Fast Fourier Transform (FFT) MATLAB routine on the thermally scaled measurements, which were obtained at a rate of 2.5 kHz in tests. The obtained FFT spectrum provides information on the bearing health status through its relevant bearing fault signature content.

The proposed method reduces the complexity of the multi-physical FBG sensing system data processing requirements and also eliminates the need for performing FBG thermal compensation, that would require additional thermal only sensors, at the expense of relative strain measurement capability. Mechanical calibration for absolute strain sensitivity determination in a bearing application is beyond the scope of this study; relative strain measurement is deemed sufficient to enable understanding of diagnostic related information. Calibrating the sensor behaviour under exclusively thermal excitation conditions however can facilitate the differentiation of in-service signatures arising

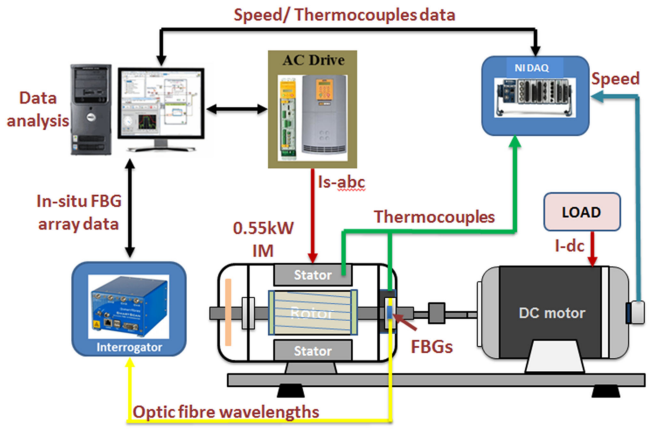


Fig. 6. Test-rig setup.

from thermal excitation from those produced by mechanical excitation, which will inherently be simultaneously registered by the in-situ sensing head.

## V. Experimental Setup and Test Operating Condition

### A. Test Rig Design

The experimental test rig system contains a three-phase 0.55kW IM driven by a Parker SDD890 drive in constant V/f control mode. For loading purposes, the IM was coupled to 0.75 kW DC permanent-magnet machine whose armature current is controlled to achieve a desired operating point. The IM three-phase voltages and current are monitored by the drive. The rotor speed is measured by an optical encoder. Fig. 6 shows a simplified schematic diagram of the used test-rig.

The FBG array sensor is interrogated by a SmartFibres SmartScan04 platform and the measurements processed using its proprietary LabView based SmartScan routine. The reflected Bragg wavelengths were acquired at a frequency of 5 kHz in the tests. For the purpose of validating the FBG bearing temperature measurements a type K thermocouple was installed on the bearing outer ring surface through a hole in the end-cap bearing housing (TC-EC). An additional thermocouple was installed at the shaft height of the test IM to monitor the ambient temperature (TC-A). The thermocouples measurements were acquired and conditioned using an NI DAQ platform (NI 9211 instrumented in NI cDAQ-9178) and LabView software.

### B. Test Operating Conditions

The developed test rig was operated at different conditions to enable the evaluation of the proposed multi-physic FBG sensing system's performance for healthy and faulty bearing condition monitoring. The IM was operated at three different supply frequencies: 50 Hz – the base frequency, 30 Hz and 10 Hz. For each considered supply frequency, three different loads were sequentially applied: no-load (NL), half-load (HL) and full-load (FL). Each examined load is maintained until reaching the IM thermal equilibrium that is then sustained for at least 1500 sec, after which the next load level is applied. The test IM was operated in the described supply and load conditions when fitted with a healthy bearing, a 0.1 mm faulty ball bearing and a 0.3 mm faulty ball bearing.

TABLE II
IM Rotor Speed (rpm) at the Examined Loads and Supply Frequencies

| | 50 Hz | 30 Hz | 10 Hz |
|---|---|---|---|
| NL | 1488 | 900 | 300 |
| HL | 1440 | 840 | 240 |
| FL | 1380 | 780 | 180 |

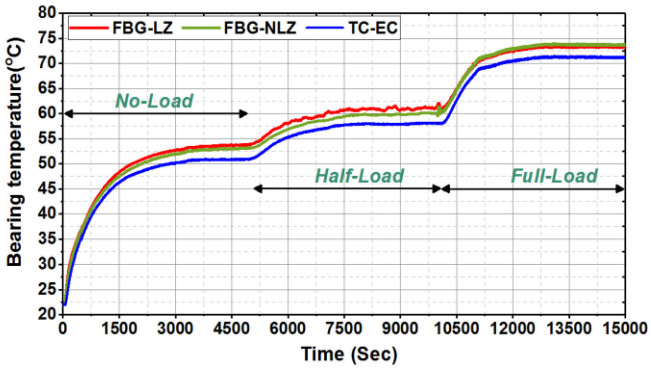


Fig. 7. Bearing temperature measurement for different loads at (50 Hz).

The applied conditions enable the emulation of different trends and levels of thermal and mechanical excitation on the examined motor design. Loading induction machines generally results in the thermal excitation increase in their components including bearings, largely caused by the associated current rise with load and the resulting winding heat loss. In contrast, loading also generally reduces the bearing mechanical excitation frequencies that are rotor speed related, as the rotor speed reduces with the increase in load. The reduction in the supply frequency will further reduce the rotor speed and thus the bearing mechanical excitation frequencies. However, low frequency operation will increase the thermal stress in the bearing structure due to the cooling system capability in the examined motor being rotor speed dependent. Table II shows the rotor speeds corresponding to particular supply frequency and load test conditions.

## VI. Experimental Results and Discussion

This section demonstrates and discusses the obtained experimental measurements of the proposed in-situ FBG sensing technique. This includes measurements obtained under healthy and faulty bearing conditions.

### A. Healthy Bearing FBG Array Sensor Measurements

*1) DC Component:* Fig. 7 shows the DC components of each FBG thermal measurement (FBG-LZ and FBG-NLZ) along with the temperature measured by the TC-EC at 50 Hz and NL, HL and FL operating conditions, following the test operating conditions set out in Section V.B. The FBG and thermocouple measurements are seen to exhibit closely similar thermal profiles, with a temperature difference of less than ≈3°C at both steady-state and transient conditions. The FBG-LZ, FBG-NLZ and the TC-EC steady-state temperature measurements for all

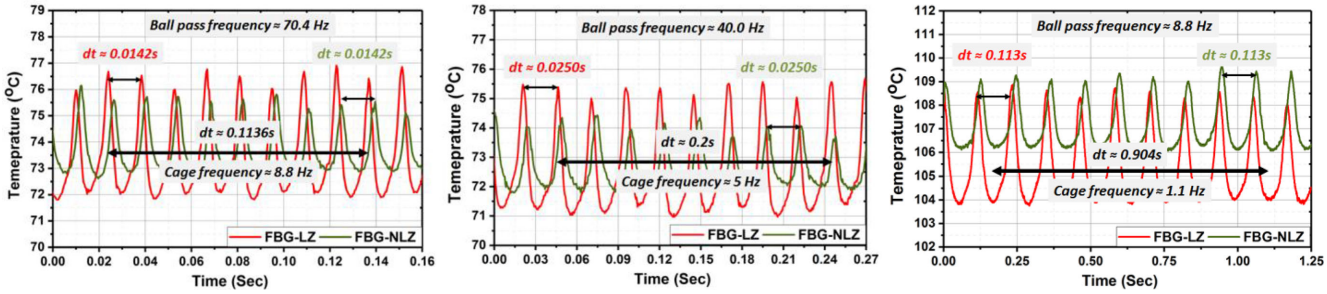


Fig. 8. In-situ FBG sensors time domain measurement taken for FL steady-state and at: (a) 50 Hz, (b) 30 Hz and (c) 10 Hz.

TABLE III
BEARING STEADY STATE TEMPERATURES

| | 50 Hz | | | 30 Hz | | | 10 Hz | | |
|---|---|---|---|---|---|---|---|---|---|
| | FBG-LZ | FBG-NLZ | TC-EC | FBG-LZ | FBG-NLZ | TC-EC | FBG-LZ | FBG-NLZ | TC-EC |
| NL | 53.8 | 53.1 | 51.2 | 53.9 | 53.9 | 50.7 | 57 | 58 | 59.2 |
| HL | 61.1 | 60 | 58.3 | 57.2 | 57.5 | 54.3 | 73.7 | 74.1 | 73.1 |
| FL | 73.4 | 73.7 | 71.2 | 72.5 | 72.4 | 70.5 | 105.1 | 107.4 | 96.57 |

examined test conditions are shown in Table III for further illustration. The consistently higher readings of FBG sensors compared to TC-EC are explained by respective sensor positions, as the TC-EC measurement is affected by the bearing housing temperature. More importantly, the good agreement between TC and FBG sensors measurements validates that the DC component of FBG measurements represents the bearing temperature.

The in-situ measurements in table III show that the bearing temperature increases with the decrease of the machine supply frequency. The reduction of the supply frequency results in decreasing the examined motor speed (refer to table II), thus reducing its cooling capability: this results in increasing the operating temperature of the motors' components including its bearings. The FBG array sensor measures an average temperature of ≈ 106 °C when motor is operated at 10 Hz and FL, which is 14 °C lower than the bearing designed permissible operating temperature [18]. Furthermore, the TC-EC reading at 10 Hz and NL in table III is seen to be higher than FBGs' readings, indicating that the heat is flowing from the end-cap to the bearing structure in these conditions. This is because at this operating condition the cooling system cannot efficiently remove the winding heat loss from the motor's frame surface, which results in dissipating the heat to cooler components such as the end caps and bearings; with load increase the rotor loss increases and is dissipated through the shaft and bearings. This changes the heat dissipation direction.

*2) AC Components:* Fig. 8(a), (b) and (c) show the FBG array time domain thermal measurements for FL steady-state conditions at 50 Hz, 30 Hz and 10 Hz supply frequency, respectively. The red and dark green traces in the figures represent the FBG-LZ and FBG-NLZ measured AC components, respectively.

The measurements obtained by FBGs exhibit a variation with a uniform pattern at each different applied excitation frequency. The observed variation can be explained by the mechanical excitation measured simultaneously with thermal excitation by the FBG sensing heads: the observed peaks in the measurement ripple are an artefact of the deformation induced in the bearing outer ring due to individual ball pass events, which is measured as in-situ strain variation by the FBG heads each time a ball passes their respective position – as the sensors' readings are converted to thermal values based on the thermal only calibration curve of the in-situ sensor these effects are manifested as high frequency ripple in the resulting thermal measurements. The experimental data demonstrate that the in-situ FBG sensor's response time is sufficient to register the relatively high frequency mechanical excitation related events in the test bearing. Furthermore, the data clearly demonstrate a magnitude variation difference between the FBG-LZ and FBG-NLZ measurements: this is observed at around 5 °C for FBG-LZ and around 3 °C for FBG-NLZ. This difference is due to the fact that the FBG-LZ is fitted in the bearing outer ring load zone and thus expected to be exposed to higher strain levels than the FBG-NLZ in the no-load zone. The test data demonstrate the high sensitivity of FBG sensors in measuring different mechanical stress levels on the bearing structure, which could provide critical information in condition monitoring applications.

The variation in the thermal measurements shown in Fig. 8 contains information on bearing operation mechanical conditions. The measured peaks frequency (FBG ball pass frequency) was found to be ≈ 70.4 Hz, ≈ 40 Hz, ≈ 8.8 Hz for 50 Hz, 30 Hz and 10 Hz, respectively. The measured frequencies closely match the test bearings manufacturer's specification of ball pass frequency value observed on the outer ring for the examined supply frequencies/speeds (70.1 Hz @ 1380 rpm, 39.6 Hz @ 1440 rpm and 9.1 Hz @ 170 rpm). The studied bearing is an eight ball design hence one full cycle of the rotating element, also known as the cage assembly rotational frequency, will generate nine successive uniformly distributed peak events at the examined speeds. The test data in Fig. 7 clearly show that the cycle time increases with frequency/speed reduction: this yields a cycle frequency of ≈ 8.8 Hz, ≈ 5 Hz and ≈ 1.1 Hz from FBGs' measurements, presenting a close match to the manufacturer data sheet values for the rotational frequency of the cage assembly (8.77 Hz @ 1380 rpm, 4.96 Hz @ 780 rpm and 1.08 Hz @ 180 rpm).

*3) FFT Analysis:* As discussed in section IV, the FFT analysis of in-situ thermal measurements could provide useful information on the bearing mechanical condition. For illustrative purposes, Fig. 9 shows the FBG-LZ and FBG-NLZ FFT spectra

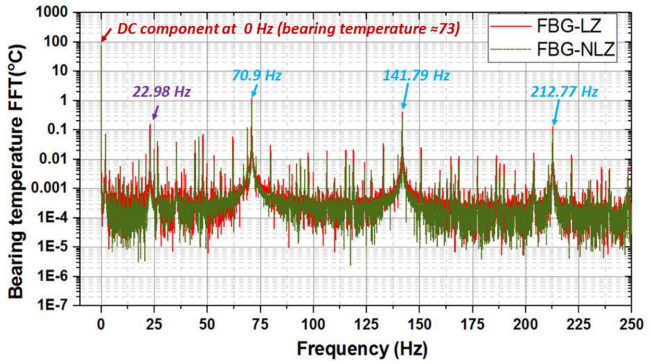


Fig. 9. FFT spectra of FBG array thermal measurement.

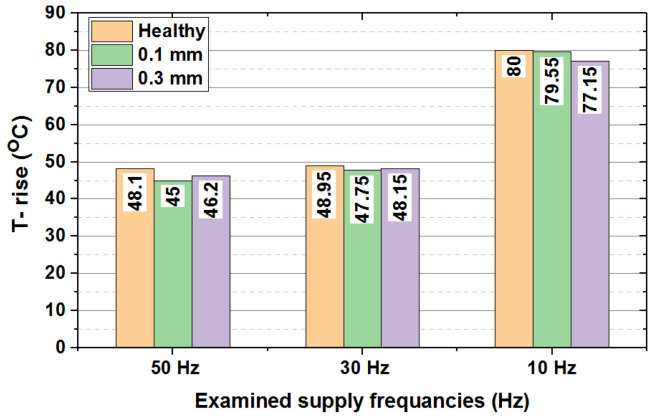


Fig. 10. In-situ measured bearing temperature rise in healthy and faulty condition.

measured at FL and 50 Hz in a frequency range of 0 250 Hz. The spectra are found to clearly report the harmonics of bearing outer ring ball pass frequencies and their multiples for each applied load/speed condition, i.e. ≈ 70.9 Hz, ≈ 141.79 Hz and ≈ 212.77 Hz etc. The thermal FFT spectra also contain harmonic components of the IM fundamental rotational speed, i.e. ≈ 22.98 Hz. Bearing temperature can also be extracted from the FFT spectra, and is represented by the DC component in the spectrum (i.e. ≈ 73.4 °C for FBG-LZ and ≈ 74.1 °C for FBG-NLZ in Fig. 9, matching the corresponding data for the examined condition in table III). The findings demonstrate that the measurements spectra contain information on both the thermal status of the bearing and its mechanical excitation conditions.

### *B. Faulted Bearing FBG Array Measurements*

To examine and evaluate the FBG sensing system capability to enable bearing fault diagnosis, a faulty ball bearing with two severity levels was emulated and tested as detailed in section II. The obtained measurements are presented and analysed in this section.

*1) DC Component:* Elevated bearing temperature is one of bearing fault signatures [3]. However, bearing temperature rise due to fault is generally expected to be significant mainly at high fault severity. For illustrative purposes, Fig. 10 shows the examined bearing temperature rise measured by the FBG array sensor in healthy and the two examined faulty ball conditions (0.1 mm and 0.3 mm) for motor operation at FL and 50 Hz, 30 Hz and 10 Hz. The presented temperature rise values are the average of FBG-LZ and FBG-NLZ measured temperatures subtracted by the measured ambient temperature. The test data show no noticeable and consistent difference between the measured bearing's temperature rise in healthy and faulty conditions. The different temperatures rise level measured at different applied frequency is due to the degradation of the motor cooling capability. The obtained thermal measurements demonstrate that at the examined low fault severity, bearing thermal signature is insufficient for effective fault detection.

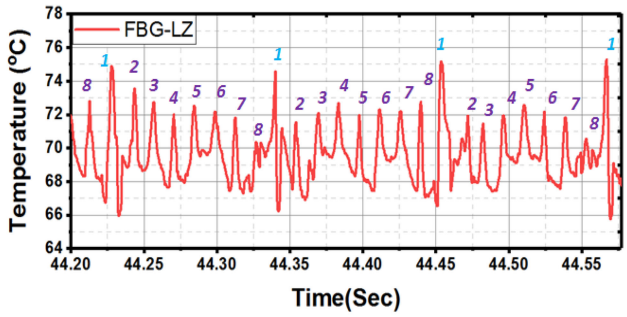


(a) FBG-LZ measurement under 0.3 mm fault condition at FL and 50 Hz.

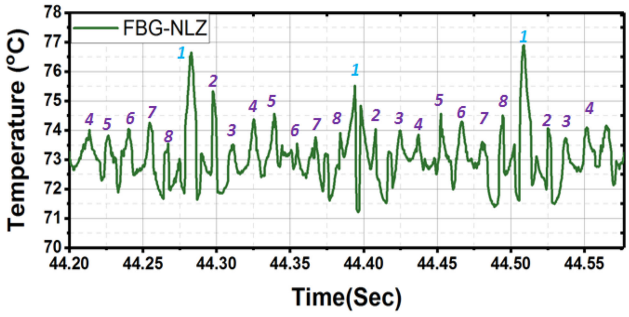


(b) FBG-NLZ measurement under 0.3 mm fault condition at FL and 50 Hz

Fig. 11. In-situ measurements' AC components analysis under damaged ball bearing conditions.

*2) AC Components:* The obtained FBG time domain measurements for the 0.3 mm ball fault at FL and 50 Hz are shown for the FBG-LZ in Fig. 11(a) and the FBG-LZ in Fig. 11(b).

The measured AC components under fault are seen to clearly change in comparison to the healthy condition (Fig. 8(a)). The individual peaks distribution in a cage cycle (numbered from 1 to 8 in Fig. 11) is seen to lose much of the relative distribution uniformity observed for a healthy bearing: the peaks have considerably different magnitude levels with one relatively high peak dominating the cycle, corresponding to the faulted ball pass event peak 1 in Fig. 11). This indicates that the outer ring deformation due to the ball pass is not uniform, which in turn indicates abnormal bearing health condition. The obtained data demonstrate that the AC component of the FBG array senor measurements can indicate the abnormality in the bearing health condition.

*3) FFT Analysis:* To further examine the fault condition related information in the obtained FBG array measurements

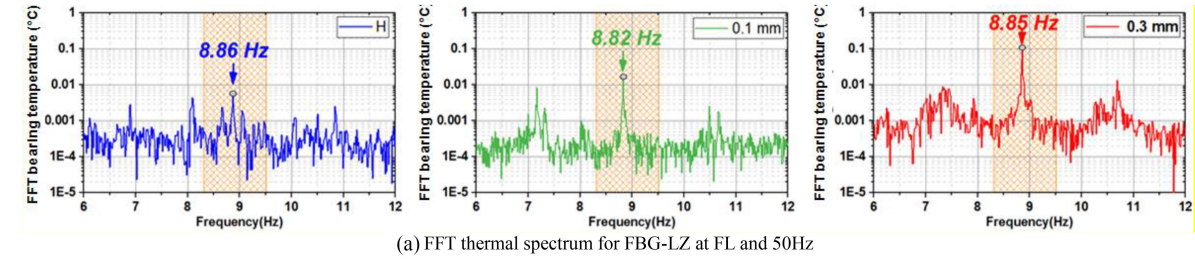


(a) FFT thermal spectrum for FBG-LZ at FL and 50Hz

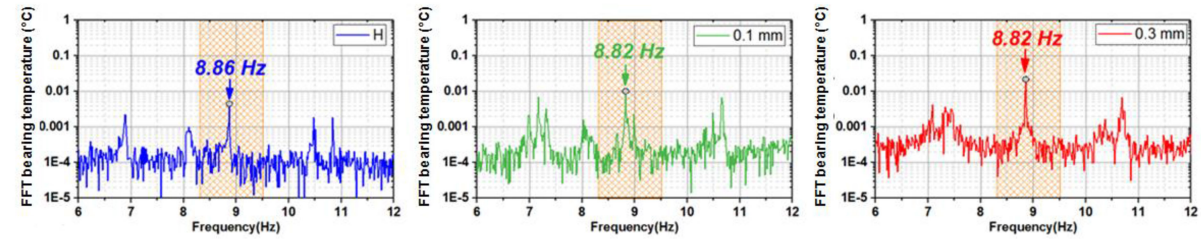


(b) FFT thermal spectrum for FBG-NLZ at FL and 50Hz

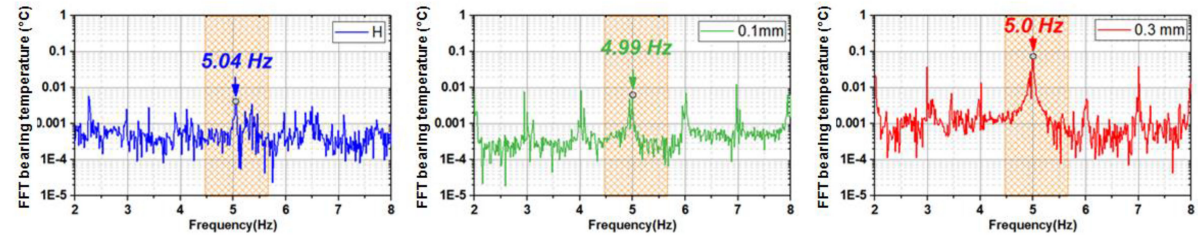


(c) FFT thermal spectrum for FBG-LZ at FL and 30Hz

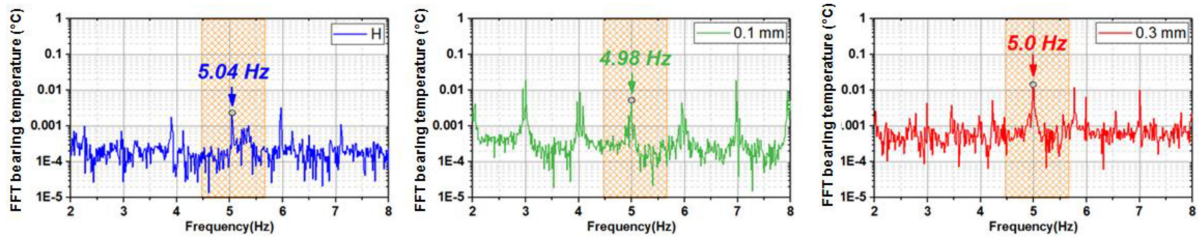


(d) FFT thermal spectrum for FBG-NLZ at FL and 30Hz

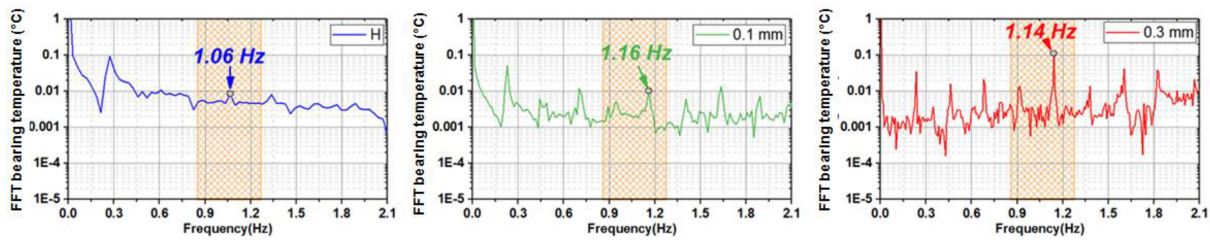


(e) FFT thermal spectrum for FBG-LZ at FL and 10Hz

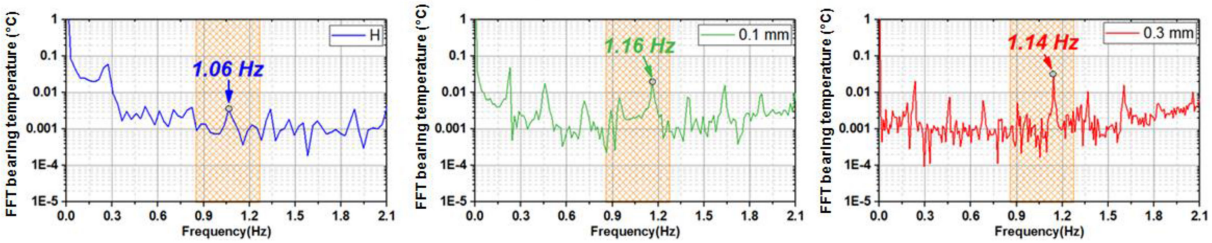


(f) FFT THERMAL SPECTRUM FOR FBG-NLZ AT FL AND 10HZ

Fig. 12. In-situ FBG measurements FFT spectra in heathy and fault conditions: healthy (blue), 0.1 mm fault (green), 0.3 mm fault (red).

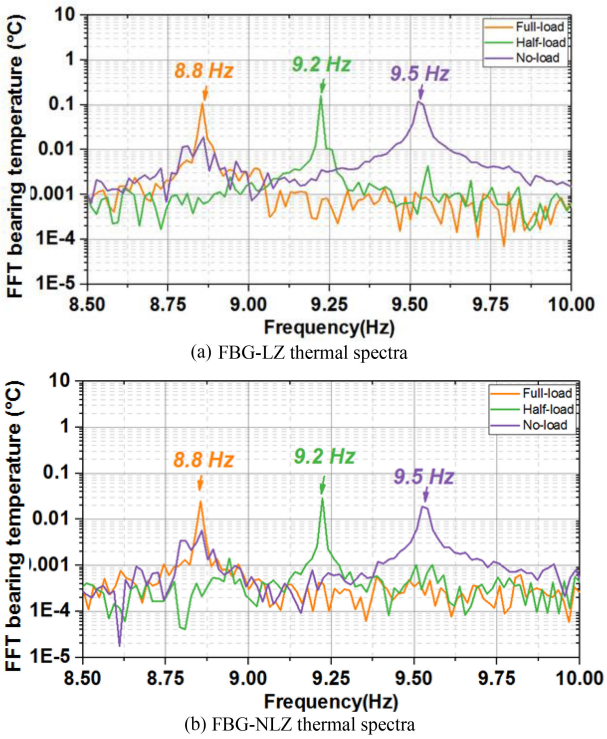


(a) FBG-LZ thermal spectra

(b) FBG-NLZ thermal spectra

Fig. 13. Thermal spectra under different loads with 0.3 mm fault.

FFT analysis was applied on the collected steady-state data for healthy and the two studied faulted ball severities. The examined single ball fault condition induces a distinct signature in the in-situ measurements spectra each time the faulty ball passes the fixed points on the outer race where FBG sensing heads are located. The specific frequency of this spectral signature is defined by dividing the bearing ball pass frequency of one point on the outer race (at the examined rotor speed) with the bearing's ball number.

For illustrative purposes, Fig. 12 shows the FBG-LZ and FBG-NLZ measured FFT spectra for FL at 50 Hz (Fig 12(a) and (b)), 30 Hz (Fig 12(c) and (d)), and 10 Hz (Fig 12(e) and (f)) supply. The FBGs spectra are presented in the narrowbands containing the fault signature frequency components. The fault frequencies are obtained by dividing the calculated ball pass frequency at the examined speed/supply frequency (70.1 Hz @ 50 Hz, 39.6 Hz @ 30 Hz and 8.64 Hz @ 10 Hz) with the ball number (8). This gives the following fault frequencies: 8.76 Hz @ 50 Hz, 4.95 @ 30 Hz and 1.08 @ 10 Hz.

The spectra in Fig. 12 are seen to clearly report the calculated fault related harmonics for each test condition. The slight difference between the calculated and the measured frequencies is due to the inherent minor deviation of the rotor speed in operation. The fault related frequency components are generally expected to appear at low magnitude in the healthy spectra (as seen in healthy (blue) traces), and are inherent to ball bearing design. The measured FFTs clearly demonstrate that the magnitude of the fault frequency component exhibits an unambiguous increase in fault presence, as illustrated by the results obtained for 0.1 mm fault (green traces) and the apparent further magnitude increase with fault severity increase (red traces, 0.3 mm case). Both FBG heads show good sensitivity to fault, however, the FBG-LZ measurements generally report higher fault magnitudes and exhibit higher sensitivity, due to their location in the bearing load zone. The presented results indicate that the FBGs's thermal measurement spectra can provide clear information on bearing fault condition. The test data also demonstrate the FBG sensing capability to register low frequency fault signatures ($<2$ Hz, as shown in Fig 12(e) and (f)). A number of nearby spectral components additional to that discussed here can also be observed in the captured spectra: while in some low supply frequency operating scenarios these can be present at reasonable magnitude level compared to the fault component, they are seen to be manifested erratically at different fault levels (such as e.g. in Fig 12(d) where their magnitude reduces with fault level increase). While borderline insignificant for nominal frequency operating conditions, similar erratic manifestation of these can at times be observed at lower supply frequency indicating that in general these components do not carry obvious diagnostic potential.

To illustrate the effect of load variation on the fault frequency component in-situ measurement Fig. 13 shows the FBG experimental spectra for the 0.3 mm ball fault condition at 50 Hz and under three different load conditions (NL, HL and FL). The data are shown in the narrow bands containing the fault frequency components for the examined load/speed conditions. The fault components are seen to manifest an almost equal magnitude for the examined loads, demonstrating that there is no obvious significant effect of load variation on the FBG sensing system performance in this application.

## VII. Conclusion

This paper explores a novel technique for electric machine healthy and faulted bearing condition monitoring utilising in-situ multi-physical fibre optic sensors. Experiments are undertaken on FBG instrumented bearings of an inverter-driven IM, by embedding sensing heads on the outer ring surface of the test motor drive end bearing, to observe its parameters in representative test studies including operation with healthy bearings and those with rolling element fault. The findings demonstrate that useful diagnostic information on both bearing mechanical and thermal operating conditions can be simultaneously extracted from a single FBG sensing head based on the proposed methodology, including clear signatures of progressive rolling element fault. The differentiation between thermal and mechanical effects is enabled by exclusively thermal calibration of the in-situ sensor prior to its in-service application, in combination with the considerably different dynamics of these two domains in rotating bearings, inherent to rotating electric machinery. It is shown that enhanced sensitivity can be achieved by sensor placement in the bearing load zone.

The presented study demonstrates that distributed single-point multi-physical monitoring of thermal and mechanical operating conditions of in-service electric machine bearings is possible utilising the reported technique. An illustrative case study of rolling element fault further demonstrates that the proposed technique can provide unambiguous monitoring and

understanding of bearing thermo-mechanical conditions during fault. The reported findings pave the way for further studies exploring a wider range of possible operating scenarios. This includes exploration of in-situ fault signatures for inner and outer race faults, but also further optimisation of monitoring sensitivity and diagnostic performance comparison with conventionally adopted monitoring techniques for electric machinery rotating bearings.

## REFERENCES


[1] P. Tavner, "Review of condition monitoring of rotating electrical machines," *Elect. Power Appl., IET*, vol. 2, pp. 215–247, 2008.

[2] P. Zhang, Y. Du, T. G. Habetler, and B. Lu, "A survey of condition monitoring and protection methods for medium-voltage induction motors," *IEEE Trans. Ind. Appl.*, vol. 47, no. 1, pp. 34–46, Jan./Feb. 2011.

[3] S. Nandi, H. A. Toliyat, and X. Li, "Condition monitoring and fault diagnosis of electrical motors—A review," *IEEE Trans. Energy Convers.*, vol. 20, no. 4, pp. 719–729, Dec. 2005.

[4] W. Zhou, T. G. Habetler, and R. G. Harley, "Bearing condition monitoring methods for electric machines: A general review," in *Proc. IEEE Int. Symp. Diagnostics Elect. Mach., Power Electron. Drives*, 2007, pp. 3–6.

[5] A. Mohammed and S. Djurović, "Stator winding internal thermal monitoring and analysis using in situ FBG sensing technology," *IEEE Trans. Energy Convers.*, vol. 33, no. 3, pp. 1508–1518, Sep. 2018.

[6] D. S. Vilchis-Rodriguez, S. Djurović, P. Kung, M. I. Comanici, and A. C. Smith, "Investigation of induction generator wide band vibration monitoring using fibre Bragg grating accelerometers," in *Proc. Int. Conf. Elect. Mach.*, 2014, pp. 1772–1778.

[7] A. Mohammed, J. I. Melecio, and S. Djurović, "Stator winding fault thermal signature monitoring and analysis by in situ FBG sensors," *IEEE Trans. Ind. Electron.*, vol. 66, no. 10, pp. 8082–8092, Oct. 2019.

[8] M. Fabian, J. Borg Bartolo, M. Ams, C. Gerada, T. Sun, and K. T. V. Grattan, "Vibration measurement of electrical machines using integrated fibre Bragg gratings," in *Proc. Int. Conf. Opt. Fibre Sensors*, 2015.

[9] A. Mohammed and S. Djurović, "FBG thermal sensing features for hot spot monitoring in random wound electric machine coils," *IEEE Sensors J.*, vol. 17, no. 10, pp. 3058–3067, May 15, 2017.

[10] M. Fabian, D. M. Hind, C. Gerada, T. Sun, and K. T. V. Grattan, "Comprehensive monitoring of electrical machine parameters using an integrated fiber bragg grating-based sensor system," *J. Lightw. Technol.*, vol. 36, no. 4, pp. 1046–1051, Feb. 15, 2018.

[11] K. M. Sousa, U. J. Dreyer, C. Martelli, and J. C. Cardozo da Silva, "Dynamic eccentricity induced in induction motor detected by optical fiber bragg grating strain sensors," *IEEE Sensors J.*, vol. 16, no. 12, pp. 4786–4792, Jun. 15, 2016.

[12] A. Mohammed, J. I. Melecio, and S. Djurović, "Open-circuit fault detection in stranded PMSM windings using embedded FBG thermal sensors," *IEEE Sensors J.*, vol. 19, no. 9, pp. 3358–3367, May 1, 2019.

[13] K. Jones, C. Staveley, and J.-F. Vialla, "Condition monitoring of a subsea pump using fibre optic sensing," in *Proc. SPIE 9157, 23rd Int. Conf. Opt. Fibre Sensors*, Jun. 2014, pp. 157–165.

[14] H. Alian, S. Konforty, U. Ben-Simon, R. Klein, and T. Moshe, "Using optical fiber sensors for health monitoring of rotational systems." in *Proc. Int. Conf. Surveillance*. 2017, pp. 1–14.

[15] P. Wei, Z. Dai, L. Zheng, and M. Li, "Fault diagnosis of the rolling bearing with optical fiber Bragg grating vibration sensor," in *Proc. SPIE. 10155, Opt. Meas. Technol. Instrum.*, Oct. 19, 2016, pp. 1–8.

[16] S. Konforty, M. Khmelnitsky, I. Kressel, R. Klein, M. Tur, and J. Bortman, "Bearing health monitoring using optical fiber sensors." in *Proc. 4th Eur. Conf. Prognostics Health Manage. Soc.*, 2016, pp. 1–7.

[17] A. Mohammed and S. Djurovic, "In-situ thermal and mechanical fibre optic sensing for in-service electric machinery bearing condition monitoring," in *Proc. IEEE Int. Elect. Mach. Drives Conf.*, San Diego, CA, USA, 2019, pp. 37–43.

[18] NSK Bearing, [Online]. Available. www.jp.nsk.com/app02/NSKOnlineCatalog